Journal of Materials Research and Technology 38 (2025) 4816–4827

Contents lists available at ScienceDirect

Journal of Materials Research and Technology

journal homepage: www.elsevier.com/locate/jmrt

Mechanical, fluoride release, and antibacterial performance of waste-derived glass ionomer cements

Zhi Wei Loh [a], Mohd Hafiz Mohd Zaid [a,b,*], Khamirul Amin Matori [a,b], Mohammad Zulhasif Ahmad Khiri [a,c], Wei Mun Cheong [a], Phey Yee Foong [d]

[a] Department of Physics, Faculty of Science, Universiti Putra Malaysia, 43400, Serdang, Selangor, Malaysia
[b] Nanomaterials Synthesis and Characterization Laboratory, Institute of Nanoscience and Nanotechnology, Universiti Putra Malaysia, 43400, Serdang, Selangor, Malaysia
[c] Material Sciences Laboratory, Department of Product Engineering, Seagate International (Johor) Sdn. Bhd., PLO55 Jalan Persiaran Teknologi, Taman Teknologi Johor, 81400, Senai, Johor, Malaysia
[d] Institute of Nano Electronic Engineering, Universiti Malaysia Perlis, Seriab, Kangar, 01000, Perlis, Malaysia

ARTICLE INFO

Handling editor: M Meyers

Keywords:
Glass ionomer cement
Ageing
Mechanical
Antibacterial
Dental restorative materials

ABSTRACT

The demand for sustainable and cost-effective dental restorative materials is growing, particularly those capable of delivering both mechanical durability and long-term bioactivity. While conventional glass ionomer cements (GICs) offer fluoride release and biocompatibility, their mechanical limitations and reliance on virgin raw materials remain concerns. This study introduces a novel approach by synthesizing GICs from recycled calcium fluoroaluminosilicate (CFAS) glass derived from glass and clamshell wastes. GIC samples were aged up to 28 days and systematically evaluated. Among the formulations, GIC-CS5 exhibited the best performance, achieving a Vickers microhardness of 275 HV and a compressive strength of 119 MPa, exceeding the ISO 9917 minimum requirement of 50 MPa. Ion chromatography revealed sustained fluoride ions ranging from 36 to 124 ppm, supporting enamel remineralization and caries prevention. Antibacterial tests against *Streptococcus mutans* showed average inhibition zones ranging from 18 to 33 mm, highlighting their potential in suppressing bacterial proliferation. These results demonstrate that waste-derived GICs can achieve competitive performance benchmarks while supporting environmental sustainability and resource efficiency in dental material development.

1. Introduction

The development of advanced dental restorative materials has been a significant area of research in biomaterials science. Among these, glass ionomer cements (GICs) have garnered widespread attention due to their inherent properties such as adhesion to tooth structure, fluoride ion release, biocompatibility, and low cytotoxicity [1–3]. Since their invention in the 1970s, GICs have evolved from conventional formulations to modified systems aiming to improve their mechanical, chemical, and biological performance [4]. These materials are primarily composed of a fluoroaluminosilicate glass powder and polyalkenoic acid, which undergo an acid-base reaction to form a hardened cement matrix [5–7]. However, traditional GICs still face limitations such as moderate mechanical strength and sensitivity to moisture during the early stages of setting [8]. In response to sustainability goals and circular economy principles, there is growing interest in utilizing waste-derived raw materials for GIC synthesis [9,10]. This approach mitigates the environmental impact of industrial and post-consumer waste and reduces reliance on virgin resources. In particular, waste glass and biogenic calcium sources such as discarded clamshells, rich in SiO_2 and CaO, can be reprocessed into calcium fluoroaluminosilicate (CFAS) glass, offering a promising alternative for GIC production. Recycled CFAS glass has shown potential to yield GICs with comparable or even improved physicochemical properties, reinforcing its relevance in restorative dentistry [11].

One of the key compositional variables in glass chemistry is calcium oxide (CaO), which not only serves as a network modifier but also facilitates the release of Ca^{2+} ions during the setting reaction [12,13]. These calcium ions are essential in crosslinking with carboxylate groups of the polyacid, contributing to the structural integrity and mechanical performance of the set cement. Moreover, CaO plays a crucial role in the crystallization of bioactive phases such as fluorapatite (FA), which

* Corresponding author. Department of Physics, Faculty of Science, Universiti Putra Malaysia, 43400, Serdang, Selangor, Malaysia.
E-mail address: mhmzaid@upm.edu.my (M.H.M. Zaid).

https://doi.org/10.1016/j.jmrt.2025.08.089
Received 19 June 2025; Received in revised form 7 August 2025; Accepted 12 August 2025
Available online 28 August 2025

Table 1
The glass formulations.

Samples	Glass formulations (in wt.%)
GIC-CS5	40SLS−5CS−15CaF_2−20Al_2O_3–20P_2O_5
GIC-CS10	35SLS−10CS−15CaF_2−20Al_2O_3–20P_2O_5
GIC-CS15	30SLS−15CS−15CaF_2−20Al_2O_3–20P_2O_5
GIC-CS20	25SLS−20CS−15CaF_2−20Al_2O_3–20P_2O_5

improves remineralization, chemical durability, and long-term bioactivity of the GICs [14]. However, excessive CaO content can alter the glass network connectivity, affect dissolution behaviour, and influence setting kinetics and ion exchange processes. Therefore, optimizing the CaO content in waste-derived GICs is critical to achieving a balance between reactivity, strength, and biofunctionality.

Ageing behaviour also plays a critical role in the evolution of the structure and performance in GICs [15,16]. Over time in aqueous environments, continued crosslinking between polyalkenoate chains and metal cations (Ca^{2+} and Al^{3+}) improves mechanical performance, while the sustained release of fluoride and calcium ions supports prolonged anticariogenic effects [17,18]. Ageing also influences microstructural transformation, including FA nucleation and particle agglomeration, which may further affect hardness, durability, and biological interaction. Despite these known effects, limited studies have systematically evaluated the age-dependent behaviour of GICs derived from recycled glass and waste materials. In addition to mechanical stability and fluoride release, antibacterial properties, especially against cariogenic bacteria like *Streptococcus mutans*, are essential for dental materials [19]. It is one of the primary cariogenic bacteria responsible for the initiation and progression of dental caries [20,21]. It is commonly found in the human oral cavity, where it metabolizes dietary sugars to produce acids that demineralize enamel [22,23]. The presence of fluoride in GICs not only facilitates remineralization but also disrupts *S. mutans* metabolism, particularly by inhibiting key glycolytic enzymes such as enolase [24,25]. The antibacterial efficacy of GICs can be influenced by factors such as ion release rate, glass composition, and pH environment. Therefore, exploring the relationship between glass formulation, fluoride release, and antibacterial activity provides valuable insights into developing multifunctional and preventive dental materials.

This study presents a cost-effective and environmentally conscious strategy for developing glass ionomer cements (GICs) using recycled calcium fluoroaluminosilicate (CFAS) glass synthesized from glass and clamshell waste. By systematically varying the CaO content in the glass formulation, the effects of compositional tuning and ageing duration on mechanical performance, fluoride ion release, and antibacterial activity were evaluated. The study also includes elemental and structural characterization to support the observed bioactive behaviour. All prepared GICs exhibited properties comparable to those stipulated in ISO 9917, reinforcing their potential clinical viability. Overall, the findings offer a sustainable pathway for valorizing waste resources into functional dental materials, aligning with global efforts toward circular economy and green material development.

2. Experimental procedure

2.1. Glass synthesis

The raw materials included CaF_2, Al_2O_3, and P_2O_5 with more than 99 % purity, whereas SiO_2 and CaO were sourced from soda lime silica (SLS) waste glass and clam shell (CS) waste, respectively. SLS glass bottles were cleaned, dried at 80 °C overnight, then crushed and milled with alumina balls at 70 rpm for 72 h. The powder was sieved through a 45 μm mesh. Raw clam shells were washed, dried at 80 °C, calcined at 900 °C for 4 h to convert $CaCO_3$ into CaO, then crushed and sieved to <45 μm, followed by preheating at 100 °C. The glass batches were formulated according to the composition [(45-*x*) SLS−*x*CS−15CaF_2–20Al_2O_3–20P_2O_5], with *x* varying from 5 to 20 wt%, as shown in Table 1. Each batch was mixed and dry-milled for 15 min, then melted at 1400 °C for 3 h. The melt was quenched in deionized water, dried at 80 °C, and ground to fine powder (<45 μm) for use in GIC formulation. Each glass composition was synthesized in triplicate under identical conditions. Repeated analysis was performed to confirm consistent glass properties for reliable GIC fabrication.

2.2. GIC preparation and ageing

Based on prior optimization studies, GICs were prepared by mixing the synthesized glass powder with polyacrylic acid (PAA) and deionized water in a fixed mass ratio of 3:1:1.2 (glass: PAA: water). The components were hand-mixed on a plexiglass plate for 60 s until homogeneous. The paste was loaded into stainless-steel cylindrical molds (6 mm height × 4 mm diameter, 9 pellets per mold), pressed between plates and cured in an oven at 37 °C for 1 h. Each GIC composition was prepared in triplicate under identical conditions to ensure reproducibility. Consistent mixing, curing, and ageing protocols were applied, with minimal variation observed across batches. After drying, the cylindrical pellet was transferred into a small bottle containing 10 ml of deionized water. This stage is called the ageing time process, and the duration of ageing times varied from 7, 14, 21, and 28 days in the electric oven at a temperature of 37 °C. Some ageing pellet samples are crushed by a plunger and sieved at 45 μm to get a fine powder for further analysis.

2.3. GIC properties

2.3.1. Physical

The density of the GIC samples was measured using an MD-300S electronic densimeter (resolution: 0.001 g/cm^3) with distilled water as the immersion liquid. Cylindrical pellets were used, and three measurements were recorded for each sample to ensure accuracy. The average of the three readings was taken as the final density value. Molar volume (V), defined as the volume occupied by 1 mol of material, was calculated using formula $V = M/\rho$, where M is the molecular mass and ρ is the measured density. This was determined for GIC samples aged at various time intervals.

2.3.2. Structural

Structural, morphological, and elemental characteristics were analyzed using complementary techniques. X-ray diffraction (XRD) was conducted using a PANalytical Philips PW 3040/60 diffractometer with CuKα radiation (λ = 1.5418 Å) over a 2θ range of 20°–80°. Phase identification was performed using X'Pert HighScore software and compared with the Powder Diffraction File (PDF) from the International Centre for Diffraction Data (ICDD). Functional groups and bonding characteristics were examined using Universal Attenuated Total Reflectance Fourier Transform Infrared Spectroscopy (UATR-FTIR; PerkinElmer Spectrum 100) in the 400–4000 cm^{-1} range at a resolution of 4 cm^{-1}. A diamond ATR crystal was used, and each spectrum was obtained by averaging 16 scans for the sample and 64 scans for the background. Raman spectroscopy was employed to complement FTIR analysis by providing vibrational mode information through inelastic scattering. Powder samples with an average particle size of 45 μm were examined using a WITec Alpha 300R Raman spectrometer. A 532 nm He–Ne laser was used as the excitation source at room temperature. Spectra were collected under ambient conditions with appropriate resolution and acquisition settings to ensure reliable detection of functional group vibrations.

Surface morphology and microstructure were examined using field emission scanning electron microscopy (FESEM; FEI NOVA NanoSEM 230) following platinum coating to minimize surface charging. Elemental composition and distribution were analyzed via energy-dispersive X-ray spectroscopy (EDX) integrated with FESEM, allowing simultaneous surface imaging and compositional analysis. All samples

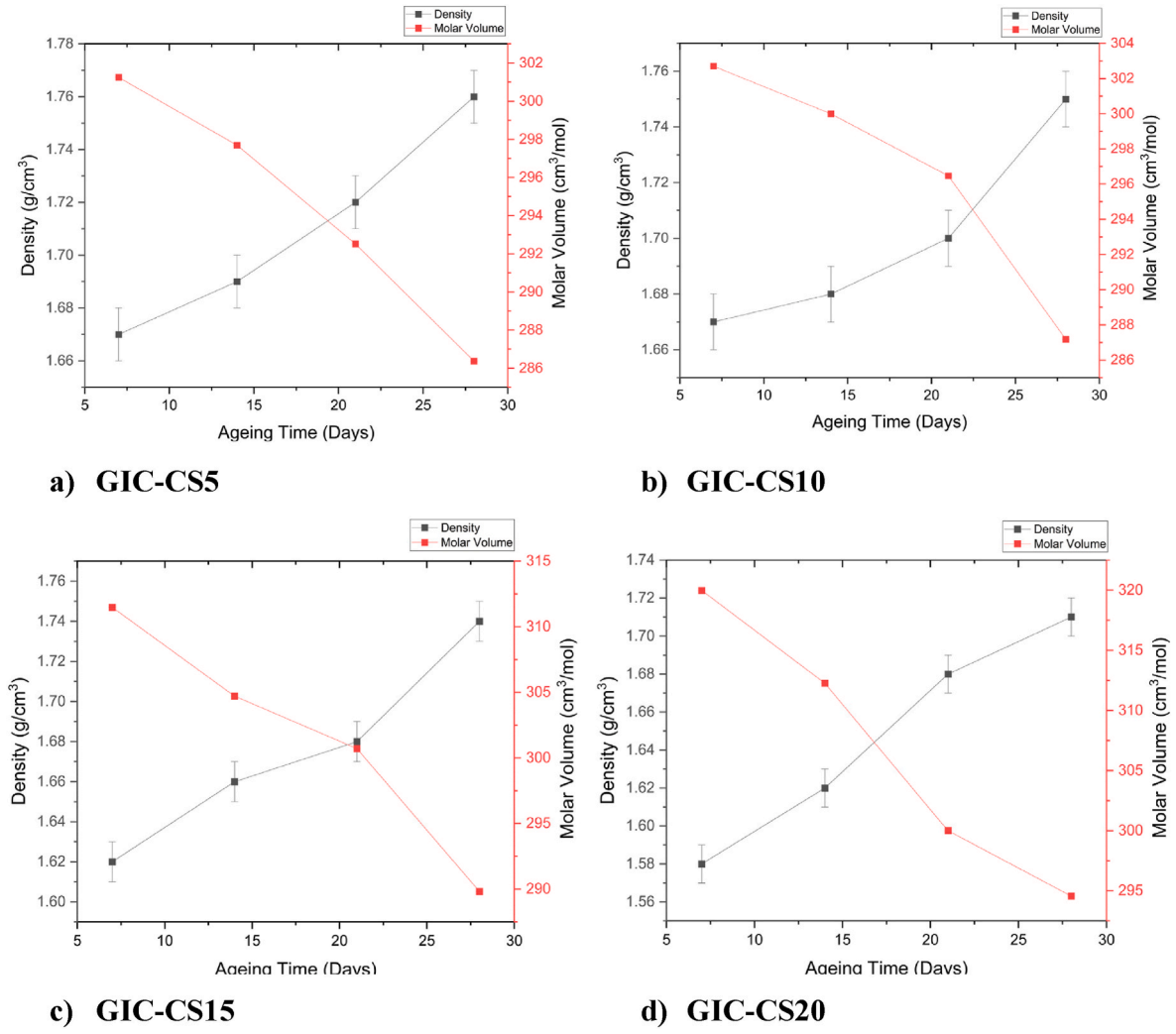

Fig. 1. Density and molar volume of GIC samples at various ageing times.

were analyzed in powder form (<45 μm), with selected polished pellets used specifically for FESEM imaging. EDX was conducted in triplicate on randomly selected areas to ensure reproducibility and minimize sampling bias. The instrument was calibrated using internal standards provided by the manufacturer. Standardless quantitative analysis was conducted under consistent operational parameters, including accelerating voltage, working distance, and detector settings. Elemental ratios, particularly Ca/P in GIC samples, were cross-validated against established literature values to confirm compositional accuracy [26–28].

2.3.3. Mechanical

The mechanical properties of the GIC samples were evaluated through Vickers microhardness and compressive strength testing. Microhardness was measured using an AVK-C2 tester (Mitutoyo, Japan) with a 0.3 kgf load and 15 s dwell time. Each pellet was polished prior to testing, and three indentations were taken per sample. Compressive strength was determined using a Universal Testing Machine (Instron 5566) at a 1.0 mm/min crosshead speed. Cylindrical GIC pellets were tested in accordance with the International Organization for Standardization standard ISO 9917–1:2025-Dentistry-Water-based cements-Part 1: Acid-base cements [29]. Five replicates were measured for each composition to ensure data reliability.

2.3.4. Antibacterial activity and fluoride ion release

The in vitro antibacterial activity of the GIC samples was assessed using the disk diffusion method against *Streptococcus mutans* (ATCC™ 25175), a key cariogenic bacterium. Bacterial cultures were prepared in Brain Heart Infusion (BHI) broth and agar under sterile conditions, with the broth sterilized at 121 °C for 15 min and adjusted to pH 7.4 ± 0.2. The bacterial suspension was standardized to 10^8 CFU/mL using a McFarland 0.5 standard. GIC pellets (5 mm diameter) were placed on agar plates seeded with bacteria and incubated at 37 °C for 24 h. Antibacterial activity was evaluated based on inhibition zone diameters, with all tests conducted in triplicate.

Fluoride ion concentration in the solution samples was determined using the Metrohm 882 Compact Inorganic Chromatography Plus system. The solutions were obtained from the ageing medium of GIC samples between 7 and 28 days. Before analysis, all solutions were filtered through a 0.2 μm pore membrane filter to eliminate particulates. The system operated under controlled pressure (11–12 MPa) and conductivity (15–16 μS/cm^2). Sodium carbonate ($NaHCO_3$, 3.2 mM) was used as the eluent, purged with helium or sonicated to remove dissolved gases and prevent microbubble formation. Sulfuric acid (H_2SO_4, 100 mM) served as the suppressor regeneration solution. Sodium fluoride (NaF, 1000 mg/L) was used as the fluoride ion reference standard. All procedures followed standard methods recommended by the American Public Health Association [30–32].

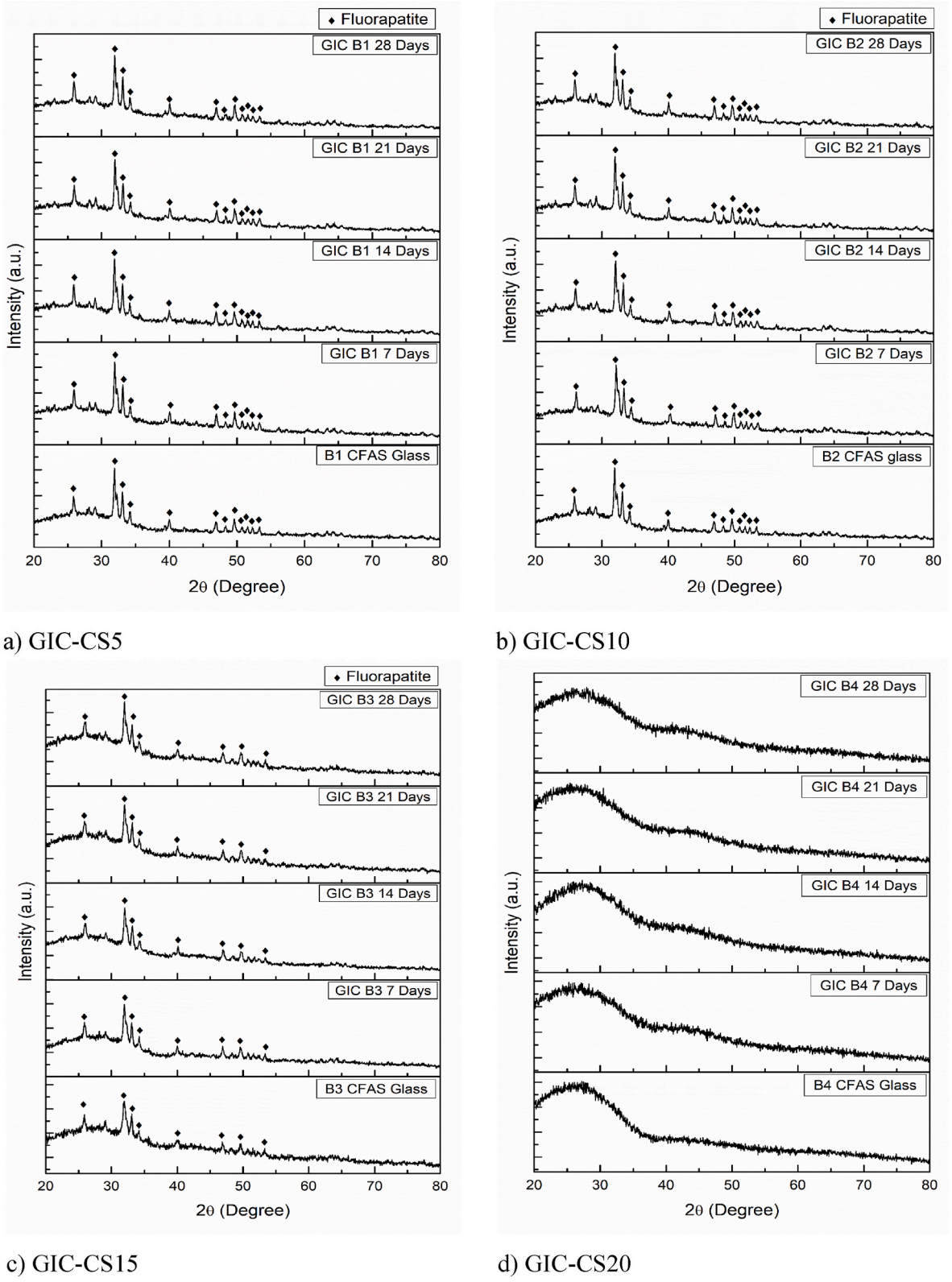

Fig. 2. XRD pattern of GIC samples with various ageing times.

3. Results and discussion

3.1. Density and molar volume

The density and molar volume values of GIC samples were measured at ageing intervals of 7, 14, 21, and 28 days, as shown in the Supplementary Table S1 and Table S2, respectively. Fig. 1 illustrates the variation in both parameters with ageing time. The density of GIC samples increased progressively with longer ageing times. This increase is attributed to the maturation and compaction of the cement matrix, accompanied by a reduction in free volume as the setting reaction proceeds. Among the samples, GIC-CS5 exhibited the highest density,

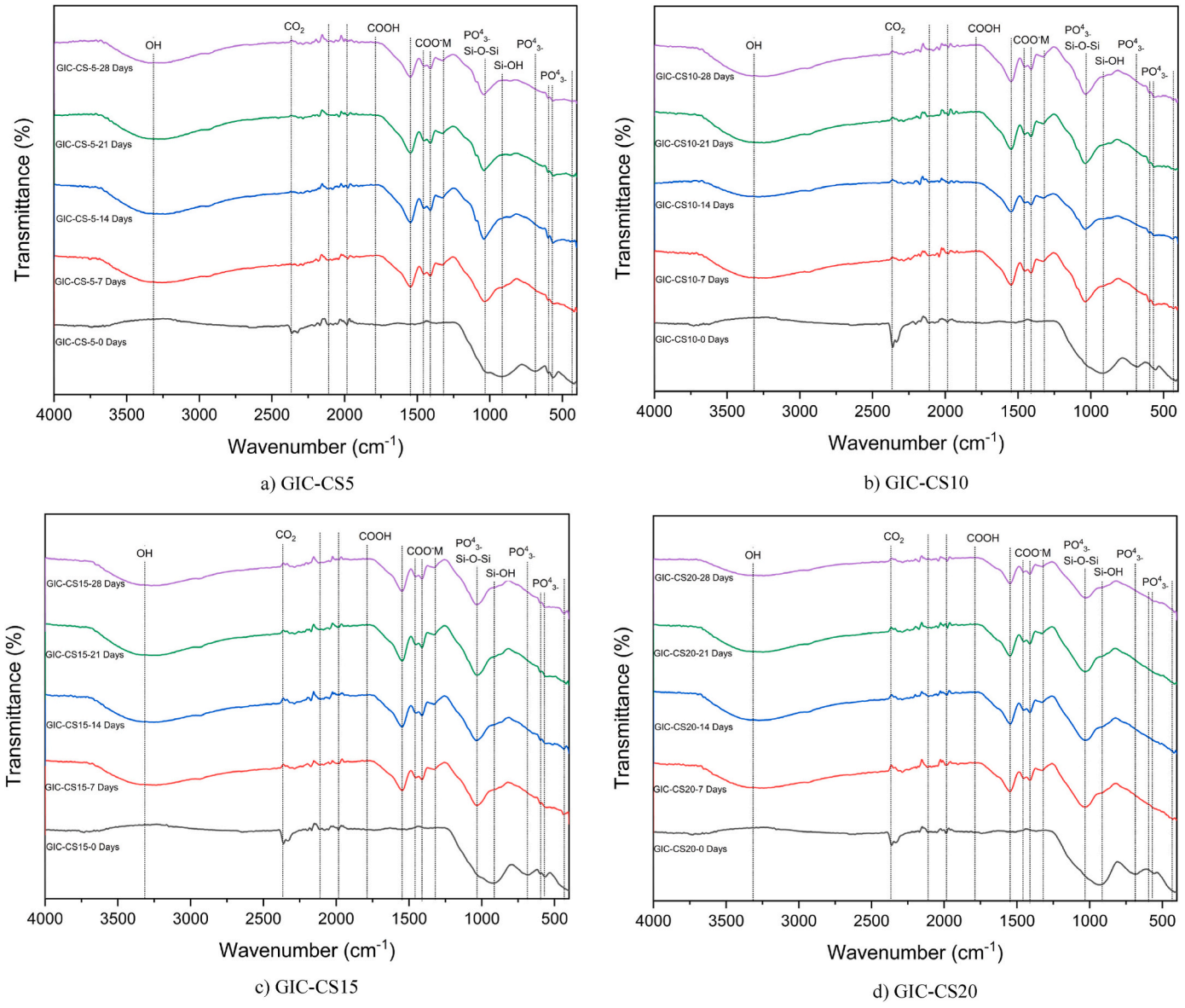

Fig. 3. FTIR spectra of GIC samples with various ageing times.

increasing from 1.67 g/cm^3 on day 7 to 1.76 g/cm^3 on day 28. The densities of GIC-CS10, GIC-CS15, and GIC-CS20 followed a similar upward trend. In contrast, the molar volume of all samples decreased over time. For GIC-CS5, the molar volume dropped from 301 cm^3/mol on day 7–286 cm^3/mol on day 28, reflecting the densification of the structure. GIC-CS20 showed the lowest initial density (1.58 g/cm^3 on day 7) and the highest initial molar volume (320 cm^3/mol). Similarly, it exhibited an increase in density and corresponding decrease in molar volume with prolonged ageing, reaching 1.71 g/cm^3 and 295 cm^3/mol, respectively, on day 28. This inverse relationship between density and molar volume is consistent with the literature, notably the findings by Ref. [33], which indicates that as materials become denser, the volume occupied per mole decreases. The densification observed here is likely linked to the formation and growth of fluorapatite (FA) crystalline phases, as supported by XRD data. Notably, the changes are more pronounced in samples with higher CaO content, suggesting that CaO acts as a nucleating agent for FA formation. Higher CaO content enhances matrix consolidation and promotes structural rearrangement, ultimately improving mechanical integrity in waste-derived GIC formulations.

3.2. XRD analysis

The XRD patterns for GIC-CS5, GIC-CS10, GIC-CS15, and GIC-CS20 are presented in Fig. 2. A progressive increase in crystalline peak intensity was observed across all compositions from 7 to 28 days of ageing, indicating the gradual formation and growth of crystalline phases over time. The primary crystalline phase identified in all samples was fluorapatite (FA), which originates from the calcium fluoroaluminosilicate glass matrix. The emergence and enhancement of FA peaks can be attributed to the inherent instability of the glass structure and the presence of CaO from the clam shell-derived component, which acts as a network modifier that promotes crystallization. Major FA peaks were observed at 2θ values of 25.86°, 28.15°, 29.08°, 31.92°, 32.26°, 33.09°, 34.15°, and 40.00°, with intensities increasing with aging time. Among the samples, GIC-CS5, GIC-CS10, and GIC-CS15 showed clear formation and growth of FA crystalline phases over the ageing period. In contrast, GIC-CS20 did not exhibit any distinct FA peaks, maintaining an amorphous halo with a gradual reduction in hump intensity, indicating densification without crystallization. This absence of FA in GIC-CS20 may be due to its higher CS content, resulting in a composition favouring amorphous network formation. The presence of FA was

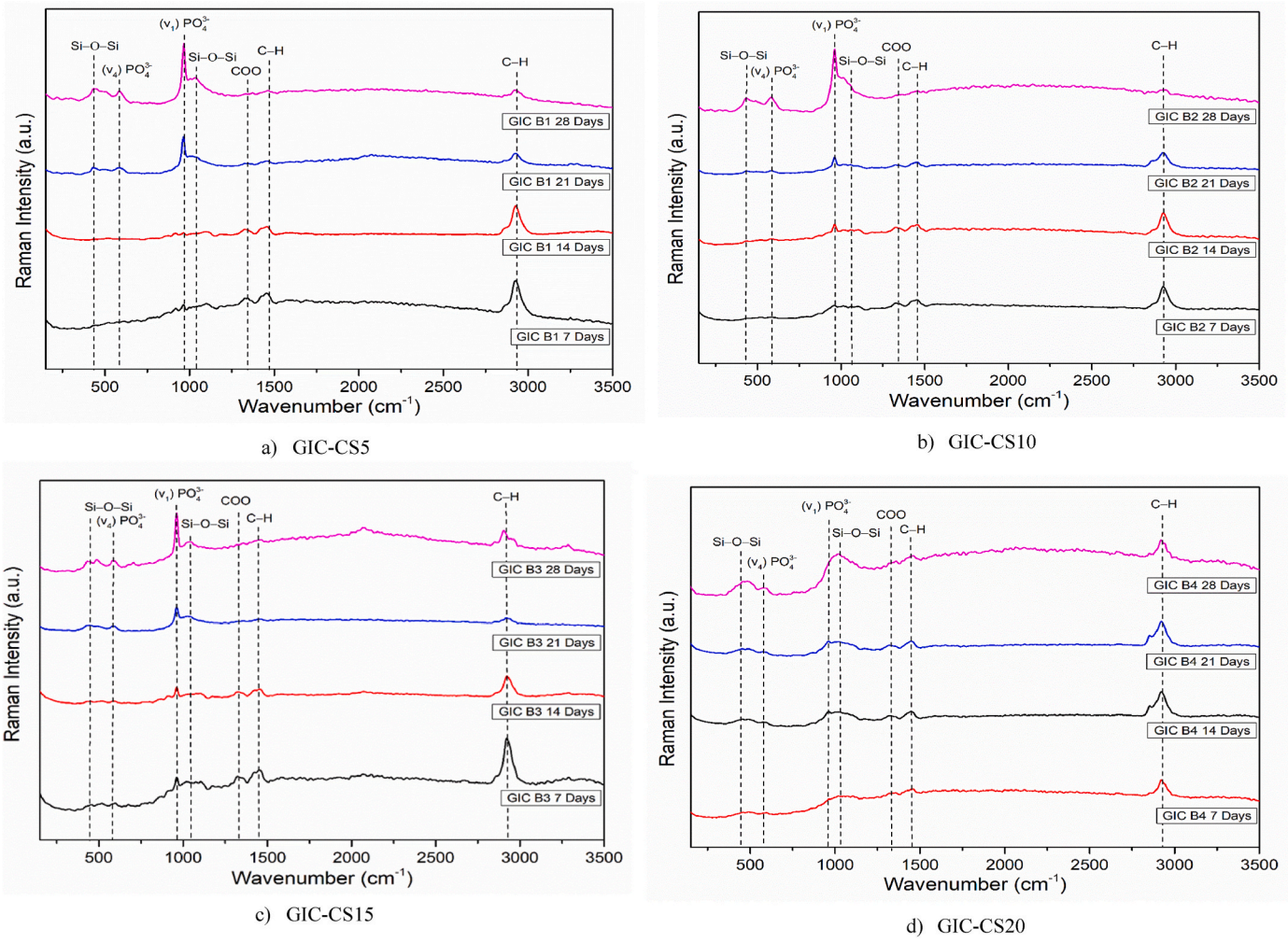

Fig. 4. Raman spectra of GIC samples with various ageing times.

further confirmed by matching the diffraction patterns with the standard reference code ICDS: 98-008-0181. Several minor FA peaks were also identified at 2θ values of 46.88°, 48.29°, 49.61°, 50.77°, 51.54°, 52.29°, 53.26°, 56.14°, 63.32°, 64.27°, and 65.44°, although their contribution to overall crystallinity was minimal. These findings confirm that ageing promotes FA crystallization in GICs with lower CS content (GIC-CS5 to GIC-CS15), while higher CS content (GIC-CS20) results in a predominantly amorphous structure. The increase in crystallinity over time is consistent with improved mechanical stability, supporting the trend observed in density and microhardness analyses.

3.3. FTIR spectroscopy

The vibrational spectra of GIC samples were analyzed using FTIR to evaluate the structural evolution from 7 to 28 days of ageing. The FTIR spectra of the base glass and GIC samples are shown in Fig. 3. All spectra were recorded in the range of 400–4000 cm^{-1}. The base glass, used to fabricate GICs, exhibited both amorphous and crystalline features depending on composition. Among the compositions, GIC-CS20 originated from a purely amorphous glass, while GIC-CS5, GIC-CS10, and GIC-CS15 showed mixed amorphous–crystalline characteristics. The base glasses exhibited three primary vibrational bands at ~566, ~923, and ~1018 cm^{-1}. The band at ~566 cm^{-1} corresponds to the asymmetric bending (v_4 mode) of PO_4^{3-} groups, characteristic of fluorapatite (FA) formation. Besides, the characteristics of the phosphate group appeared at around 460 cm^{-1}, 692 cm^{-1} and 1024 cm^{-1} corresponding to the asymmetric bending (v_4), symmetric (v_1) and asymmetric (v_3) stretching vibrational modes, respectively. The Si–OH symmetric bending (~923 cm^{-1}) and Si–O–Si asymmetric stretching (~1018 cm^{-1}) is associated with the silicate network and indicate the presence of both amorphous and crystalline silicate structures. Weaker bands at ~460, ~800, ~2360, and ~3435 cm^{-1} were also observed. The band at ~2360 cm^{-1} is assigned to CO_2 asymmetric stretching, attributed to incomplete decomposition of $CaCO_3$ from clam shell-derived CaO, while the broad band at ~3435 cm^{-1} arises from O–H stretching due to adsorbed moisture.

During GIC formation, an acid–base reaction occurs between the polyacrylic acid (PAA) and base glass in an aqueous medium. The hydronium ions from PAA attack the glass particles, releasing Al^{3+}, Ca^{2+}, and F^- ions. These cations interact with carboxylate groups (COO^-) from PAA, forming a polysalt matrix. In the initial stage, a strong vibrational band at ~1700 cm^{-1} corresponding to COOH groups was observed. As ageing progresses, this band diminishes due to ionization into COO^- and H^+, and new bands emerge at ~1550–1589 cm^{-1}, representing metal–carboxylate complexes (COO–M^{n+}, where M = Ca^{2+} or Al^{3+}). Additional features include a weak band at ~1405 cm^{-1}, attributed to symmetric stretching of reacted COO–M^{n+} groups. This reflects the ongoing coordination reactions of COO^- with Ca^{2+} and Al^{3+} during the ageing period. Overlapping of bands in the 1400–1600 cm^{-1} region complicates differentiation between calcium and aluminum carboxylate species, which may be influenced by steric hindrance and incomplete ionization of PAA. In summary, FTIR spectra of GIC-CS5 to GIC-CS20 revealed consistent acid–base reaction behaviour with increasing ageing time, confirming the progressive formation of a polysalt matrix

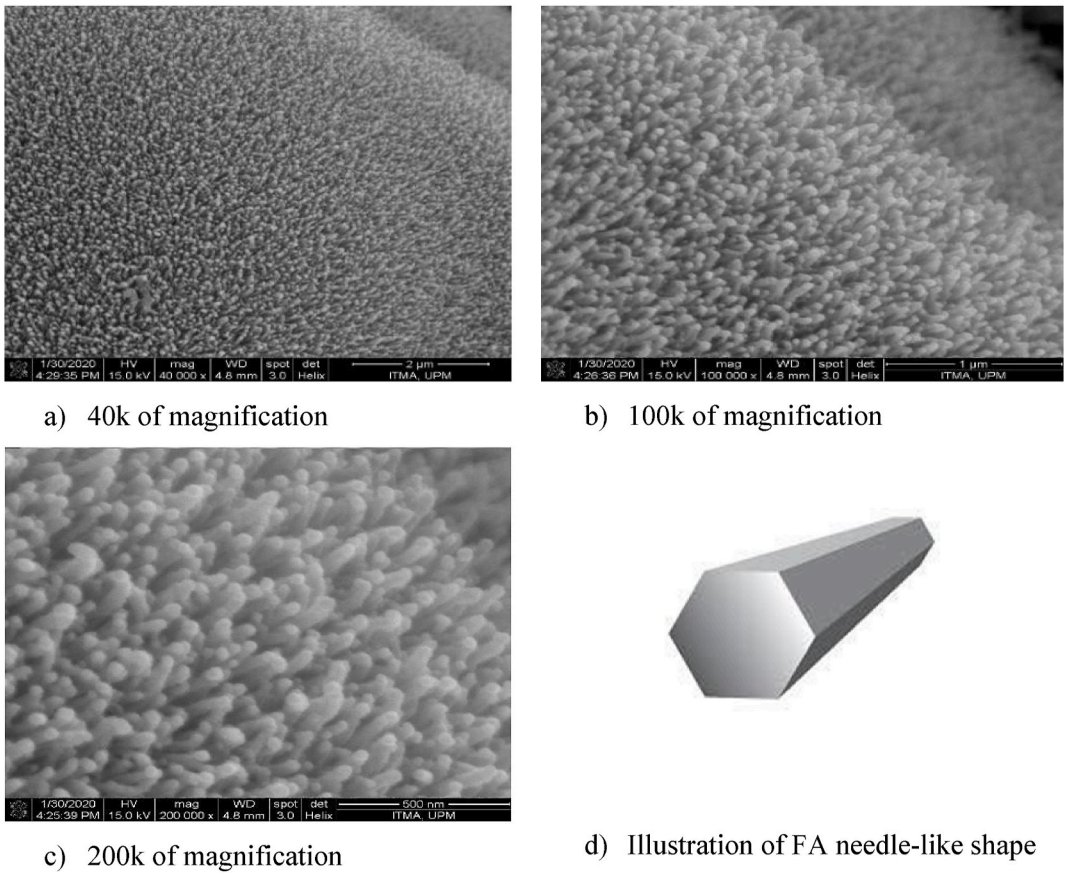

Fig. 5. FESEM micrograph of GIC-CS5 at 28 days of ageing time.

and changes in the structural bonding environment. These spectral evolutions support the observed physical and mechanical property changes during GIC maturation. A summary of the key FTIR bands observed in GIC samples is provided (See Supplementary Table S3).

3.4. Raman spectroscopy

The Raman spectra of GIC samples were analyzed to assess structural changes from 7 to 28 days of ageing. Samples GIC-CS5, GIC-CS10, and GIC-CS15 displayed prominent features associated with the fluorapatite (FA) crystalline phase, consistent with XRD results. GIC-CS20, composed of a fully amorphous glass, exhibited no FA-related peaks throughout the ageing process. The Raman spectra are presented in Fig. 4, and the summary of vibrational modes and corresponding assignments is tabulated in Table S4 (See Supplementary Section).

Across all the samples, seven characteristic Raman bands were observed at ~431, ~582, ~950, ~1000, ~1328, ~1456, and ~2924 cm^{-1}, corresponding to vibrational modes originating from both the glass and polyacrylic acid (PAA). The Si–*O*–Si symmetric and asymmetric stretching modes, identified at ~431 and ~1000 cm^{-1} respectively, increased in intensity with ageing. This trend indicates the progressive condensation of Si–OH to Si–*O*–Si linkages, consistent with the FTIR analysis. Raman bands at ~582 cm^{-1} (ν_4 PO_4^{3-} bending) and ~950 cm^{-1} (ν_1 PO_4^{3-} symmetric stretching) were attributed to phosphate units in the FA crystalline phase. Their increased intensity with ageing, particularly in GIC-CS5 to GIC-CS15, confirmed the gradual development of FA. The ν_1 PO_4^{3-} band at ~950 cm^{-1} was especially distinct and served as a reliable indicator of FA growth. The vibrational features at ~1328, ~1456, and ~2924 cm^{-1} were associated with PAA-related functional groups. The ~1328 cm^{-1} band, attributed to symmetric COO^- stretching or CH_2 twisting, decreased with ageing time due to coordination of COO^- groups with mobile cations (Ca^{2+} and Al^{3+}) released from the glass matrix. This coordination supports the formation of a stable cross-linked polysalt matrix, as also evidenced in FTIR analysis. The Raman bands at ~1456 and ~2924 cm^{-1} were assigned to C–H_2 and C–H stretching modes. The ~1456 cm^{-1} band corresponds to C–H_2 deformation and was observed as a weak feature across all samples. Its intensity diminished with ageing, reflecting the neutralization process occurring during the acid–base reaction between PAA and the glass. The ~2924 cm^{-1} band, corresponding to C–H or CH_2 stretching, exhibited strong intensity across all GIC samples but showed inconsistent behaviour over time.

In general, the Raman signal for this vibration decreased with extended ageing, which is attributed to the continuing neutralization and interaction of free CH_2/C–H groups with mobile ions in the aqueous environment surrounding the glass particles. Overall, the Raman analysis confirmed structural evolution within GIC samples, particularly the growth of FA crystallinity and progression of the acid–base reaction network.

3.5. FESEM-EDX

The surface morphology and elemental distribution of GIC samples were examined using Field Emission Scanning Electron Microscopy (FESEM) equipped with Energy-Dispersive X-ray Spectroscopy (EDX). Representative micrographs and corresponding elemental mappings for various ageing times (7–28 days) are presented in Fig. 6. FESEM analysis revealed the presence of fluorapatite (FA) crystalline phases across all samples, except GIC-CS20. For GIC-CS5, GIC-CS10, and GIC-CS15, distinct nanoscale particles were observed on the surface, exhibiting predominantly spherical morphologies when viewed perpendicular to the sample plane. Given that the FA phase is known to crystallize in a

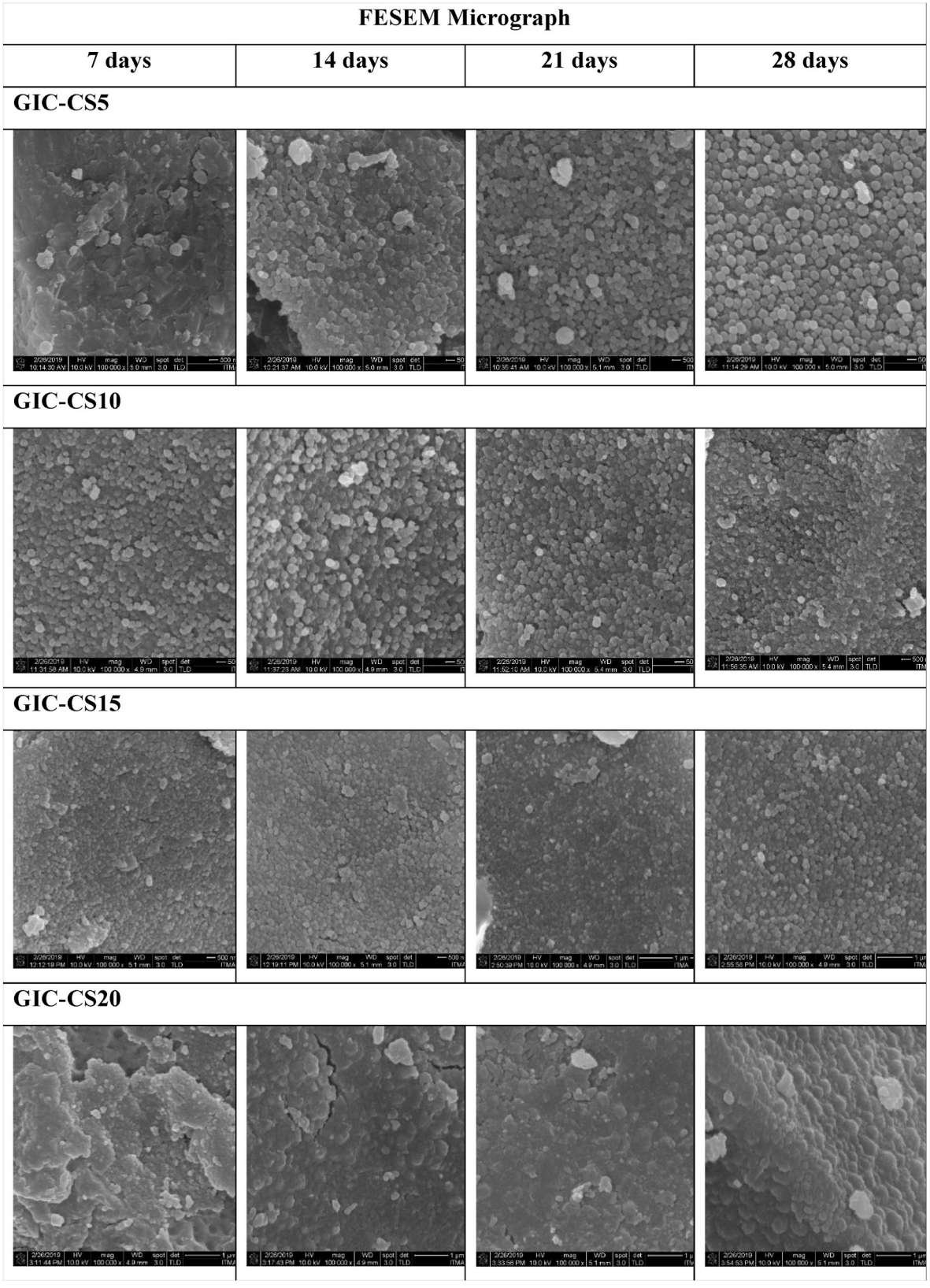

Fig. 6. FESEM micrograph of GIC samples at various ageing times.

hexagonal system, an additional angled FESEM view (<90° tilt) was employed to capture cross-sectional features of the surface (Fig. 5).

This perspective confirmed the presence of hexagonal, needle-like, and spherical particles characteristic of FA crystals, consistent with ref. [34–36]. The observed FA crystallites appear to grow via heterogeneous nucleation on existing particles, leading to the formation of clustered, oriented aggregates. Such needle-like clusters are particularly evident in GIC-CS5 to GIC-CS15 across all ageing times.

Table 2
Vickers microhardness and compressive strength of GIC samples at various ageing times.

GIC samples	Vickers Microhardness (HV)			
	7 days	14 days	21 days	28 days
GIC-CS5	116 ± 11	139 ± 12	204 ± 19	275 ± 28
GIC-CS10	145 ± 14	147 ± 14	151 ± 15	166 ± 17
GIC-CS15	102 ± 10	137 ± 13	139 ± 14	147 ± 14
GIC-CS20	69 ± 7	75 ± 7	86 ± 9	121 ± 11
GIC samples	**Compressive Strength (MPa)**			
	7 days	**14 days**	**21 days**	**28 days**
GIC-CS5	46 ± 5	51 ± 5	80 ± 8	104 ± 10
GIC-CS10	55 ± 5	76 ± 7	86 ± 9	100 ± 9
GIC-CS15	57 ± 5	74 ± 8	82 ± 8	94 ± 9
GIC-CS20	46 ± 4	57 ± 5	78 ± 8	88 ± 9

Notably, GIC-CS20 displayed a predominantly amorphous surface with no distinct crystalline features, in agreement with XRD data showing the absence of FA formation. Additionally, significant particle agglomeration was observed in all GIC samples due to electrostatic interactions between FA crystallites, resulting in densely packed domains across the sample surfaces. These findings further support the presence and evolution of FA during the ageing process and align with compositional changes detected via EDX elemental mapping.

The size of fluorapatite (FA) particles in GIC samples was estimated using FESEM micrographs analyzed with ImageJ software. The analysis focused exclusively on measuring the tip diameter of the needle-like FA crystals, as the full particle length was difficult to determine due to overlapping structures and unclear boundaries. The average particle sizes at various ageing times are summarized in Fig. S1 (See Supplementary Section). The overall average size of the FA particle in the GICs consistently ranged between 50 and 90 nm, with a predominant average around ~60 nm in every batch composition of GIC. This uniform particle size distribution suggests stable nucleation and growth behaviour of FA crystallites during the ageing process, regardless of composition or duration.

The elemental composition of GIC samples at various ageing times was determined using EDX, and the results are presented in Table S5 (See Supplementary Section). All samples contained O, F, Na, Mg, Al, Si, P, Ca, and C. Oxygen was the most abundant element, with weight percentages ranging from 24.9 wt% to 43.5 wt%, attributed to the predominance of oxide constituents in the CFAS glass formulation. Ca, Al, Ca, and Si were also present in significant amounts, originating from the base glass network. To evaluate the bioactive potential of the samples, the Ca/P and (Ca + Mg)/P ratios were calculated based on the elemental weight percentages. The Ca/P ratio ranged from 1.02 to 3.95 across all GIC-CS compositions (GIC-CS5, GIC-CS10, GIC-CS15, and GIC-CS20), while the (Ca + Mg)/P ratio, which accounts for the isomorphic substitution potential of Mg^{2+} in calcium phosphate structures, ranged from 1.07 to 3.99. According to Refs. [37–39], materials with a Ca/P ratio greater than 1 are generally considered suitable for biomedical implant applications. The inclusion of Mg further supports the potential for phosphate-based crystallite formation, such as fluorapatite (FA), which was also observed in SEM micrographs.

Of particular note, GIC-CS5 at 21 days exhibited a sharp increase in the Ca/P ratio, which may be attributed to inhomogeneous ion migration or localized reprecipitation of calcium-rich phases. While no significant morphological differences were observed in the corresponding FESEM micrograph, it is possible that Ca^{2+} ions accumulated in specific surface regions, leading to the formation of submicron Ca-phosphate domains not easily detected within the imaging field. The elemental distribution thus becomes non-uniform at this time point, despite the sample's overall chemical stability. Such behavior aligns with the ongoing maturation processes in GICs, during which ionic exchange and crystallization can persist beyond the initial setting.

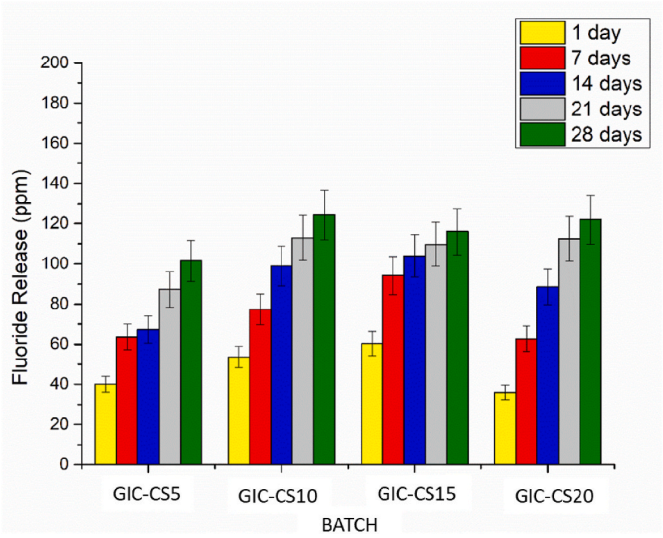

Fig. 7. Fluoride ions released by ion chromatography of the GIC samples at various ageing times.

These findings indicate that the GIC samples exhibit compositional characteristics conducive to bioactivity. Nonetheless, additional biocompatibility assessments and in vitro/in vivo evaluations are required to confirm their suitability for dental clinical applications.

3.6. Vickers microhardness

The average Vickers microhardness of GIC samples was evaluated across ages 7, 14, 21, and 28 days, as presented in Table 2. All batches (GIC-CS5, GIC-CS10, GIC-CS15, and GIC-SC20) consistently increased microhardness over time. Notably, GIC-CS5 showed the most significant improvement, rising from 116 HV at 7 days to 275 HV at 28 days. GIC-CS10 increased from 145 HV to 166 HV, GIC-CS15 from 102 HV to 147 HV, and GIC-CS20 from 69 HV to 121 HV over the same period. These results suggest continued maturation of the cement matrix due to ongoing crosslinking reactions and water-mediated hydration, which strengthen the polysalt network over time. As confirmed by XRD and FESEM analyses, GIC-CS5 contains well-developed fluorapatite (FA) crystalline phases that act as reinforcing entities within the matrix, enhancing mechanical strength. In contrast, the predominantly amorphous structure of GIC-CS20, with limited or no FA crystallization, results in reduced mechanical reinforcement. These findings underscore the importance of controlled crystallization and network evolution in optimizing the long-term mechanical stability of waste-derived GIC formulations.

3.7. Compressive strength

The compressive strength of GIC samples was assessed over ageing times of 7, 14, 21, and 28 days (Table 2). All formulations demonstrated a consistent increase in compressive strength over time, indicating ongoing maturation and ionic crosslinking within the cement matrix. At 7 days, GIC-CS5 exhibited a compressive strength of 46 MPa, which increased significantly to 104 MPa by 28 days. Similarly, GIC-CS10 improved from 55 MPa to 100 MPa, GIC-CS15 from 57 MPa to 94 MPa, and GIC-CS20 from 46 MPa to 88 MPa over the same period. Among all, GIC-CS5 recorded the highest compressive strength after 28 days, which can be attributed to the formation of well-defined fluorapatite (FA) crystallites. The FA crystalline phase reinforces the cement network, enhancing its mechanical integrity and load-bearing capacity. In contrast, GIC-CS20, which maintained a predominantly amorphous structure, exhibited comparatively lower strength due to the lack of crystalline reinforcement.

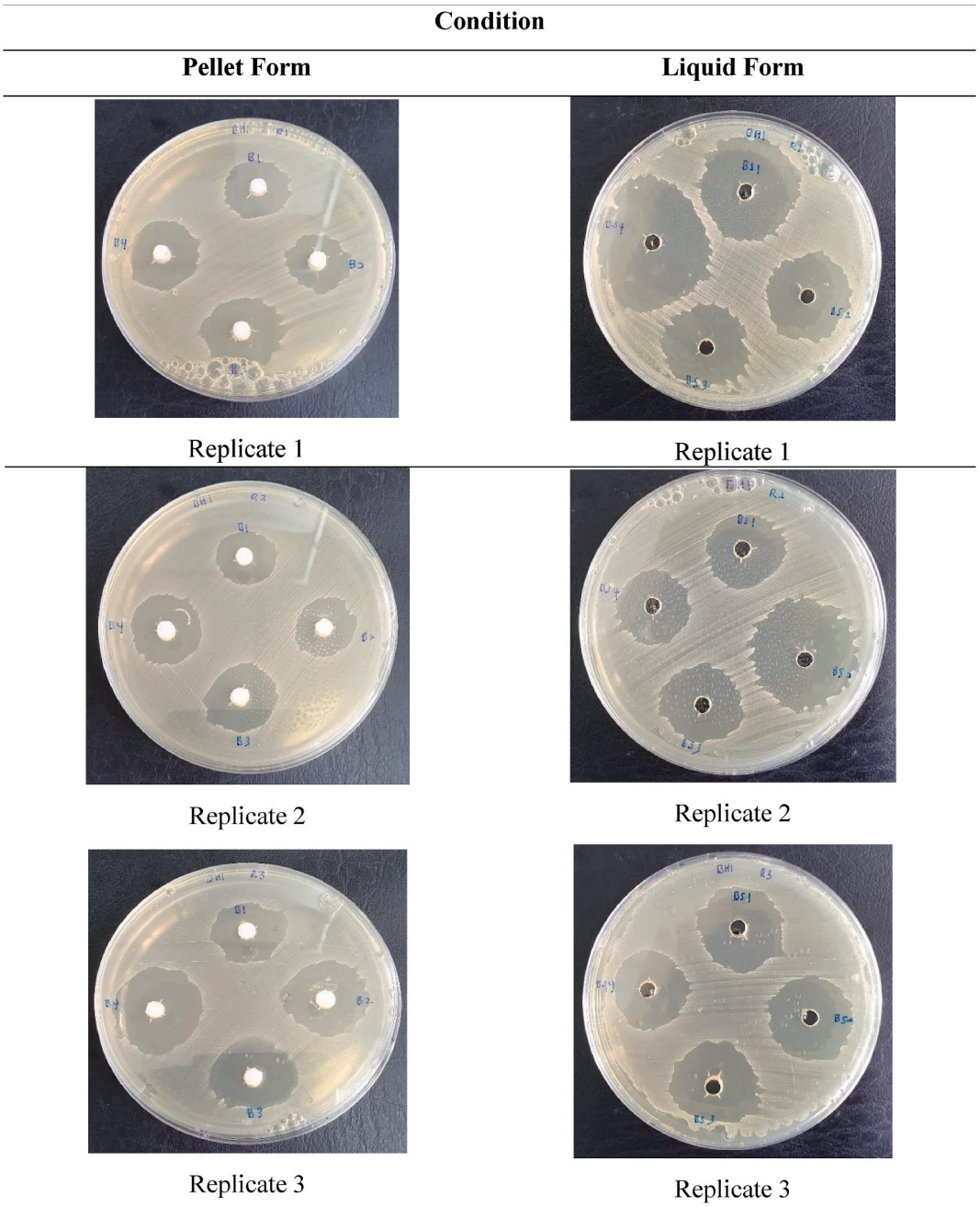

Fig. 8. The inhibition zone of GIC samples under different conditions by the disk diffusion method.

The observed trend is in line with previous studies showing that compressive strength increases with ageing as metal ions (Ca^{2+}, Al^{3+}) from the glass react progressively with carboxylate groups in the polyacid to form a robust ionic crosslinked network. Additionally, the polymerization of silanol groups (Si–OH) into siloxane bonds (Si–*O*–Si) contributes to network densification and hardening over time. According to ISO 9917 standards for water-based dental cements, a minimum compressive strength of 50 MPa is required for clinical applications, which all formulations surpassed after 28 days of ageing.

3.8. Fluoride release

Fluoride ion release from GIC samples was evaluated using ion chromatography over 1, 7, 14, 21, and 28 days of ageing. The fluoride ion concentrations released into the soaking medium are presented in Table S6 (See Supplementary Section) and illustrated in Fig. 7. All GIC samples demonstrated a progressive increase in fluoride release with extended ageing time. GIC-CS5 exhibited a release of 40 ppm at 1 day, increasing to 101 ppm at 28 days. Similarly, fluoride ion concentrations for GIC-CS10 rose from 54 to 124 ppm, for GIC-CS15 from 60 to 116 ppm, and for GIC-SC20 from 36 to 122 ppm over the same period. This consistent upward trend confirms the sustained fluoride-releasing capability of GICs developed from the base glass.

Interestingly, GIC-CS20, which retained a predominantly amorphous structure throughout the ageing period, exhibited relatively higher fluoride ion release. This is attributed to the disordered and porous nature of the amorphous phase, which provides a larger surface area and facilitates rapid diffusion and dissolution of fluoride ions into the surrounding medium. In contrast, GIC-CS5, GIC-CS10, and GIC-CS15 demonstrated progressive FA crystallization, as confirmed by

increasing peak intensities in XRD patterns. Fluoride ions incorporated into the stable hexagonal FA lattice are less readily leached, contributing instead to a slower, sustained release via surface dissolution and ion exchange.

Thus, the degree of crystallinity plays a key role in governing fluoride release kinetics [40]. Amorphous phases enable higher initial ion mobility, while crystalline phases act as long-term fluoride reservoirs. This balance between structure and release mechanism enhances the therapeutic efficacy of GICs by supporting both immediate and prolonged cariostatic effects [41,42]. The multifunctional role of the glass matrix in modulating these behaviours reinforces its potential in sustainable, bioactive dental applications.

3.9. Antibacterial activity

The antibacterial properties of GIC samples were evaluated against *Streptococcus mutans* using the disk diffusion method under two test conditions: pellet form and ageing solution form (28 days). The aim was to assess the ion diffusion efficacy and its inhibitory effect on oral bacteria. Representative images of the disk diffusion assay are presented in Fig. 8. Fresh GIC samples were tested for direct fluoride release into the agar medium in the pellet form.

As shown in Table S7 (See Supplementary Section), the average inhibition zone diameters against *S. mutans* ranged from 19 to 24 mm across GIC-CS5 to GIC-SC20. GIC-SC20 exhibited the widest inhibition zone (24 mm), indicating more potent antibacterial activity. The observed inhibition corresponds to fluoride ion release, which is crucial in suppressing bacterial proliferation. The release of fluoride, Ca^{2+}, Al^{3+}, and OH^{-} ions around the pellet is believed to reduce the pH, contributing to bacterial inhibition [43]. This aligns with earlier findings that fluoride [42], especially in the form of hydrofluoric acid (HF), can penetrate bacterial membranes, dissociate intracellularly, and disrupt enzymatic processes essential to bacterial metabolism, primarily by inhibiting the enolase enzyme, thereby impairing phosphoenolpyruvate (PEP) production and ultimately stunting bacterial growth [44–46].

GIC ageing solutions at 28 days were tested for the solution form to verify their antibacterial potential. As shown in Table S8 (See Supplementary Section), the inhibition zones were generally wider compared to the pellet form, ranging from 25 to 28 mm. GIC-SC20 again demonstrated the highest antibacterial activity with a zone of 28 mm. The enhanced performance in liquid form can be attributed to more efficient fluoride ion diffusion, allowing greater interaction with the agar medium and more effective inhibition of *S. mutans* growth. These results affirm the sustained antibacterial potential of glass-based GIC, with the ageing solution further enhancing ion mobility and bacterial suppression.

4. Conclusion

This study presents a sustainable and cost-effective strategy for developing multifunctional glass ionomer cements (GICs) using recycled calcium fluoroaluminosilicate glass derived from glass and clamshell waste. Among the formulations, GIC-CS5 demonstrated the highest performance, achieving a Vickers microhardness of 275 HV and compressive strength of 119 MPa, exceeding ISO 9917 standards. Structural analyses confirmed the formation of fluorapatite (FA) crystallites, contributing to the material's bioactivity and long-term stability. Meanwhile, ion chromatography revealed sustained fluoride release (36–124 ppm) across all samples. Antibacterial testing against *Streptococcus mutans* showed inhibition zones of 18–33 mm, underscoring the materials' potential in caries prevention. These findings collectively highlight the potential of waste-derived GICs to serve as environmentally responsible, clinically viable restorative dental materials. Further in vivo and long-term biocompatibility studies are warranted to advance their translational application.

CRediT authorship contribution statement

Zhi Wei Loh: Conceptualization, Formal Analysis, Investigation, Software, Visualization, Writing – Original Draft. **Mohd Hafiz Mohd Zaid:** Data curation, Funding acquisition, Project administration, Supervision, Validation, Writing – Original Draft. Khamirul Amin Matori: Data curation, Supervision, Validation, Writing – review & editing. **Mohammad Zulhasif Ahmad Khiri:** Conceptualization, Formal Analysis, Investigation, Writing – Original Draft. **Wei Mun Cheong:** Resource, Software, Visualization, Writing – review & editing. **Phey Yee Foong:** Software, Validation, Writing – review & editing.

Declaration of competing interest

The authors declare that they have no known competing financial interests or personal relationships that could have appeared to influence the work reported in this paper.

Acknowledgements

This research was supported by the Universiti Putra Malaysia via the Geran Putra Inisiatif (GPI/2023/9762700) for this research.

Appendix A. Supplementary data

Supplementary data to this article can be found online at https://doi.org/10.1016/j.jmrt.2025.08.089.

References

[1] Kabir A, Rahman M, Kabir H, Khan M. Effect of hydroxyapatite filler in an aluminosilicate glass ionomer cements. J Mater Sci Chem Eng 2025;13:83–98. https://doi.org/10.4236/msce.2025.132006.
[2] Jain K, Paulraj J, Maiti S, Shanmugam R. Green synthesis and investigation of antimicrobial activity and compressive resilience of Glass Ionomer cement modified with Zirconia nanoparticles: an In vitro study. Cureus 2024;16. https://doi.org/10.7759/cureus.62837.
[3] Lathikumari SS, Saraswathy M. Ionogel impregnated glass ionomer cement and the effect of nanoparticle additives. Mater Adv 2024:7432–45. https://doi.org/10.1039/d4ma00592a.
[4] Ge KX, Yu-Hang Lam W, Chu CH, Yu OY. Updates on the clinical application of glass ionomer cement in restorative and preventive dentistry. J Dent Sci 2024. https://doi.org/10.1016/j.jds.2024.07.021.
[5] Gjorgievska E, Nicholson JW, Gabrić D, Guclu ZA, Miletić I, Coleman NJ. Assessment of the impact of the addition of nanoparticles on the properties of glass-ionomer cements. Materials 2020;13:1–12. https://doi.org/10.3390/ma13020276.
[6] Alobiedy AN, Alhille AH, Al-Hamaoy AR. Mechanical properties enhancement of conventional glass ionomer cement by adding zirconium oxide micro and nanoparticles. J Eng 2019;25:72–81. https://doi.org/10.31026/j.eng.2019.02.05.
[7] Sasidharan Lathikumari S, Saraswathy M. Modifications of polyalkenoic acid and its effect on glass ionomer cement. Mater Adv 2024;5:2719–35. https://doi.org/10.1039/d3ma00406f.
[8] Azimi R, Shahgholi M, Khandan A. Fabrication and characterization of reinforced glass ionomer cement by zinc oxide and hydroxyapatite nanoparticles. Heliyon 2024;10:e39063. https://doi.org/10.1016/j.heliyon.2024.e39063.
[9] Khiri MZA, Matori KA, Zaid MHM, Abdullah AC, Zainuddin N, Jusoh WNW, et al. Soda lime silicate glass and clam shell act as precursor in synthesize calcium fluoroaluminosilicate glass to fabricate glass ionomer cement with different ageing time. J Mater Res Technol 2020;9:6125–34. https://doi.org/10.1016/j.jmrt.2020.04.015.
[10] Osiro OA, Tiskaya M, Shahid S, Hill RG. Evaluation of dental cements derived from mixtures of highly reactive ionomer glasses and bottle glass: cement manipulation, mechanical, fluoride ion releasing, radiopaque and setting properties. Dent Mater 2024;40:1981–90. https://doi.org/10.1016/j.dental.2024.09.013.
[11] Wan Jusoh WN, Matori KA, Zaid MHM, Zainuddin N, Khiri MZA, Rahman NAA, et al. Incorporation of hydroxyapatite into glass ionomer cement (Gic) formulated based on alumino-silicate-fluoride glass ceramics from waste materials. Materials 2021;14:1–14. https://doi.org/10.3390/ma14040954.
[12] Thongsri O, Srisuwan S, Thaitalay P, Dangwiriyakul R, Aengchuan P, Chanlek N, et al. Structural evaluation of ZnO substitution for CaO in glass ionomer cement synthesized by sol-gel method and their properties. J Mater Sci 2022;57:633–50. https://doi.org/10.1007/s10853-021-06517-6.
[13] Vilela HS, Resende MCA, Trinca RB, Scaramucci T, Sakae LO, Braga RR. Glass ionomer cement with calcium-releasing particles: effect on dentin mineral content and mechanical properties. Dent Mater 2024;40:236–43. https://doi.org/10.1016/j.dental.2023.11.005.

[14] Tsolianos I, Nikolaidis AK, Koulaouzidou EA, Achilias DS. An evaluation of experimental calcium ion-leachable nanocomposite Glass ionomer cements. Nanomaterials 2023;13:1–20. https://doi.org/10.3390/nano13192690.
[15] Ratajski J, Bałasz B, Mydłowska K, Pancielejko M, Szparaga Ł. The effect of ageing on phase transformations and mechanical behaviour in Ni-Rich NiTi alloys. Materials 2024;17. https://doi.org/10.3390/ma17102420.
[16] Pai Y, Dayananda Pai K, Vijaya Kini M. Effect of ageing conditions on the low velocity impact behavior and damage characteristics of aramid-basalt/epoxy hybrid interply composites. Eng Fail Anal 2023;152:107492. https://doi.org/10.1016/j.engfailanal.2023.107492.
[17] Madi F, Sidhu SK, Nicholson JW. The effect of temperature and ionic solutes on the fluoride release and recharge of glass-ionomer cements. Dent Mater 2020;36:e9–14. https://doi.org/10.1016/j.dental.2019.11.018.
[18] Rufasto-Goche KS, Cerro-Olivares ES, Martín-Hilario NS, Santander-Rengifo FM, Murillo-Carrasco AG, Lizarbe-Castro MV. Fluoride-Induced microhardness changes in resin-modified glass ionomer cements: a comparative study. J Clin Exp Dent 2025;17:e50–7. https://doi.org/10.4317/jced.62349.
[19] Gunay A, Celenk S, Adiguzel O, Cangul S, Ozcan N, Cakmakoglu EE. Comparison of antibacterial activity, cytotoxicity, and fluoride release of glass Ionomer restorative dental cements in dentistry. Med Sci Monit 2022;28:1–8. https://doi.org/10.12659/MSM.939065.
[20] Al-Khalifa KS, Alsheikh R, Al-Hariri MT, El-Sayyad H, Alqurashi MS, Ali S, et al. Evaluation of the antimicrobial effect of thymoquinone against different dental pathogens: an in vitro study. Molecules 2021;26:1–10. https://doi.org/10.3390/molecules26216451.
[21] Kashi M, Varseh M, Hariri Y, Chegini Z, Shariati A. Natural compounds: new therapeutic approach for inhibition of Streptococcus mutans and dental caries. Front Pharmacol 2025;16:1–20. https://doi.org/10.3389/fphar.2025.1548117.
[22] Zayed SM, Aboulwafa MM, Hashem AM, Saleh SE. Biofilm formation by Streptococcus mutans and its inhibition by green tea extracts. AMB Express 2021;11. https://doi.org/10.1186/s13568-021-01232-6.
[23] Gao Z, Chen X, Wang C, Song J, Xu J, Liu X, et al. New strategies and mechanisms for targeting Streptococcus mutans biofilm formation to prevent dental caries: a review. Microbiol Res 2024;278:127526. https://doi.org/10.1016/j.micres.2023.127526.
[24] Mahendra TVD, Rahul TS, Ramesh KSV, Pasupuleti S, Velagala SK, Mulakala V. Quantitative determination and antibacterial properties of TiO2 nanoparticle-doped glass ionomer cement: an in vitro study. Eur Oral Res 2024;58:8–13. https://doi.org/10.26650/eor.20231225662.
[25] Nicholson JW, Sidhu SK, Czarnecka B. Fluoride exchange by glass-ionomer dental cements and its clinical effects: a review. Biomater Investig Dent 2023;10. https://doi.org/10.1080/26415275.2023.2244982.
[26] Putranto AW, Meidyawati R, Dwiseptyoga S, Zikrullah DYA. Evaluation of physical properties in Carboxymethyl Chitosan modified Glass ionomer cements and the effect for dentin remineralization: SEM/EDX, compressive strength, and Ca/P ratio. Eur J Dent 2024;19:187–96. https://doi.org/10.1055/s-0044-1786864.
[27] Ramić B, Cvjetićanin M, Bajkin B, Drobac M, Milanović M, Rajnović D, et al. Physical and mechanical properties assessment of glass ionomer cements modified with TiO2 and Mgdoped hydroxyapatite nanoparticles. J Appl Biomater Funct Mater 2024;22. https://doi.org/10.1177/22808000241282184.
[28] El-Hamid HKA, Hamzawy EMA, Nagi SM, Elwan RL. Effect of modification of glass ionomer cement restorations by low-cost soda-lime-silica glass/tetracalcium phosphate composites. Ceram Int 2025;51:6947–58. https://doi.org/10.1016/j.ceramint.2024.12.129.
[29] International Organization for Standarization. ISO 9917-1:2025-Dentistry-Water-based cements-part 1: Acid-base cements. 2025.
[30] Tolkou AK, Manousi N, Zachariadis GA, Katsoyiannis IA, Deliyanni EA. Recently developed adsorbing materials for fluoride removal from water and fluoride analytical determination techniques: a review. Sustain Times 2021;13. https://doi.org/10.3390/su13137061.
[31] Anwar H, Sisca V, Siregar EP, Elizarni Subriadi F, Elfina S. Validation of the use of ion chromatography for analysis of fluoride in water. Rasayan J Chem 2024;17:868–74. https://doi.org/10.31788/RJC.2024.1738800.
[32] Rice EW, Baird RB, Eaton AD. Standard methods for the examination of water and wastewater. 23rd Edition 2017.
[33] Al-Ghamdi H, Alsaif NAM, Nabil IM, Abdelghany AM, Rammah YS, Abouhaswa AS. Strontium oxide-reinforced borotellurite glasses: synthesis, structure, and optical characteristics and γ-Ray and neutron attenuation capability. J Electron Mater 2024;53:5647–62. https://doi.org/10.1007/s11664-024-11201-x.
[34] Fiume E, Magnaterra G, Rahdar A, Verné E, Baino F. Hydroxyapatite for biomedical applications: a short overview. Ceramics 2021;4:542–63. https://doi.org/10.3390/ceramics4040039.
[35] Chen H, Sun Q, Zhang J, Sheng J. Effect of MgF2 addition on sinterability and mechanical properties of fluorapatite ceramic composites fabricated by wollastonite and phosphate glass. Ceram Int 2022;48:20400–8. https://doi.org/10.1016/j.ceramint.2022.03.325.
[36] Jusoh WNW, Matori KA, Zaid MHM, Zainuddin N, Khiri MZA, Rahman NAA, et al. Effect of sintering temperature on physical and structural properties of alumino-silicate-fluoride glass ceramics fabricated from clam shell and soda lime silicate glass. Results Phys 2019;12:1909–14. https://doi.org/10.1016/j.rinp.2019.01.077.
[37] Roslan Z, Amin KM, Zaid MHM, Yaakob Y, Kul E, Loh ZW, et al. Investigating the influence of CaO/CaF2 ratios on the synthesis of calcium-alumino-silicate-fluoride-based glass ceramics utilizing recyclable materials. Appl Phys A Mater Sci Process 2024;130. https://doi.org/10.1007/s00339-024-08053-x.
[38] Hou X, Zhang L, Zhou Z, Luo X, Wang T, Zhao X, et al. Calcium phosphate-based biomaterials for bone repair. J Funct Biomater 2022;13. https://doi.org/10.3390/jfb13040187.
[39] Mishchenko O, Yanovska A, Kosinov O, Maksymov D, Moskalenko R, Ramanavicius A, et al. Synthetic calcium–phosphate materials for bone grafting. Polymers 2023;15:1–49. https://doi.org/10.3390/polym15183822.
[40] Panah NG, Atkin R, Sercombe TB. Bioactivity and biodegradability of high temperature sintered 58S ceramics. J Eur Ceram Soc 2022;42:3614–23. https://doi.org/10.1016/j.jeurceramsoc.2022.02.051.
[41] Tiwari S, Kenchappa M, Bhayya D, Gupta S, Saxena S, Satyarth S, et al. Antibacterial activity and fluoride release of glass-ionomer cement, compomer and zirconia reinforced glass-ionomer cement. J Clin Diagnostic Res 2016;10:ZC90–Z93. https://doi.org/10.7860/JCDR/2016/16282.7676.
[42] Farooq I, Hassan U, Mahdi S, Ullah R, Rana H. Newer glass ionomer cements having strontium ions and the effect of their release on acidic medium. Int J Prosthodont Restor Dent 2012;2:57–60. https://doi.org/10.5005/jp-journals-10019-1049.
[43] Bagchi A, Dolker T, Talukdar A, Sowmya K, Khan MM, Raj U. An in vitro study on the antibacterial efficiency of the various composites in the children: an original research. J Pharm BioAllied Sci 2023;5:S192–5. https://doi.org/10.4103/jpbs.JPBS.
[44] Pradiptama Y, Purwanta M, Notopuro H. Antibacterial effects of fluoride in Streptococcus mutans growth in vitro. Biomol Heal Sci J 2019;2:1. https://doi.org/10.20473/bhsj.v2i1.13232.
[45] Liao Y, Brandt BW, Li J, Crielaard W, Van Loveren C, Deng DM. Fluoride resistance in Streptococcus mutans: a mini review. J Oral Microbiol 2017;9. https://doi.org/10.1080/20002297.2017.1344509.
[46] Morawska-Wilk A, Kensy J, Kiryk S, Kotela A, Kiryk J, Michalak M, et al. Evaluation of factors influencing fluoride release from dental nanocomposite materials: a systematic review. Nanomaterials 2025;15:1–18. https://doi.org/10.3390/nano15090651.